

# Prediction-Based Approaches for Generation of Noise-Power-Distance Data with Application to Urban Air Mobility Vehicles

Stephen A. Rizzi\*, Stefan J. Letica†, D. Douglas Boyd, Jr.‡, and Leonard V. Lopes§  
NASA Langley Research Center, Hampton, VA 23681, USA

**In contrast to most commercial air traffic today, vehicles serving the urban air mobility (UAM) market are anticipated to operate within communities and be close to the public at large. The approved model for assessing environmental impact of air traffic actions in the United States, the Federal Aviation Administration (FAA) Aviation Environmental Design Tool (AEDT), does not directly support analysis of such operations due to a combined lack of UAM aircraft flight performance model data and aircraft noise data. This paper addresses the latter by offering two prediction-based approaches for generation of noise-power-distance (NPD) data for use within AEDT. One utilizes AEDT’s fixed-wing aircraft modeling approach and the other utilizes the rotary-wing aircraft modeling approach.**

## I. Introduction

**I**N the United States, the Federal Aviation Administration (FAA) Aviation Environmental Design Tool (AEDT)<sup>1</sup> is the required tool to assess aircraft noise and other environmental impacts due to federal actions at civilian airports, vertiports, or in U.S. airspace for commercial flight operations. AEDT and prediction tools with the same or similar modeling technologies are used in other countries as well.<sup>2</sup> For fixed-wing aircraft, AEDT calculates various noise metrics using noise-power-distance (NPD) data specific to each aircraft. In its customary mode of operation, the AEDT flight performance model determines the engine power required to execute the specified flight operation. A key assumption is that noise levels are highly correlated with the corrected net thrust of the engines. This allows noise data to be interpolated for power and distance, along with various other adjustments, to estimate the sound exposure at a set of receptors on the ground. For rotary-wing aircraft (helicopters), AEDT calculates sound exposure using noise-operational mode-distance (still termed NPD) data specific to the vehicle’s operational mode, e.g., vertical ascent. The noise data are interpolated for distance only and are used, with adjustments, to estimate the sound exposure at a set of ground receptors. There is no equivalent correlating parameter such as corrected net thrust.

There are some obstacles to using AEDT for assessment of community noise due to urban air mobility (UAM) vehicle operations. The first is that while there are NPD data for existing fixed-wing and rotary-wing vehicles in the databases used in AEDT, there are no available NPD data for UAM vehicles, whether the vehicles are modeled as fixed-wing or rotary-wing type vehicles. Secondly, when modeling a UAM vehicle as a fixed-wing type, there are no performance data available to determine required engine power, nor is it clear that engine power is a good predictor of noise. When modeling a UAM vehicle as a rotary-wing type, the number of defined operating modes within AEDT are limited to a few that are appropriate for typical helicopter operations but that may be insufficient for describing UAM operations.

A recent white paper<sup>3</sup> established a set of high-level goals to address key issues associated with UAM noise. One of these goals is to examine UAM fleet noise impacts through prediction and measurement, along with a recommendation that “*Research be conducted to more fully explore limitations in methods for assessing community noise impact of UAM vehicles in their operational environments, and to generate a software development plan that addresses the limitations of current models over time.*” To that end, this paper describes two approaches for generating UAM vehicle NPD data for use in AEDT. Both approaches are based on source noise predictions using the NASA second-generation Aircraft Noise Prediction Program (ANOPP2).<sup>4</sup> One approach is directed at generating NPD data suitable for modeling UAM vehicles as fixed-wing types in AEDT. The other approach is

---

\* Senior Researcher for Aeroacoustics, Aeroacoustics Branch, [stephen.a.rizzi@nasa.gov](mailto:stephen.a.rizzi@nasa.gov), AIAA Fellow

† Research Engineer, Aeroacoustics Branch, [stefan.j.letica@nasa.gov](mailto:stefan.j.letica@nasa.gov)

‡ Senior Research Engineer, Aeroacoustics Branch, [d.d.boyd@nasa.gov](mailto:d.d.boyd@nasa.gov), AIAA Senior Member

§ Senior Research Engineer, Aeroacoustics Branch, [leonard.v.lopes@nasa.gov](mailto:leonard.v.lopes@nasa.gov)

directed at generating NPD data for modeling UAM vehicles as rotary-wing types in AEDT. The first generation (Gen 1) fixed-wing NPD database contained periodic loading and thickness noise for two UAM reference vehicles.<sup>5</sup> The second generation (Gen 2) fixed-wing NPD database added broadband self noise.<sup>6</sup> In this work, updates to the Gen 2 source noise data serve as the basis for a third generation (Gen 3) NPD database for fixed-wing and rotary-wing type vehicles.

## II. Concept Vehicles and Operating States

### A. Vehicle Description

Two reference vehicles developed under the NASA Revolutionary Vertical Lift Technology (RVLT) Project are included in this investigation, namely, the quadrotor and lift plus cruise (L+C) vehicles, see Figure 1. Both vehicles are sized for a 1200 lb. payload (up to six passengers) executing a representative mission profile.<sup>7</sup> The quadrotor is an all-electric variant, with four three-bladed rotors, gross weight of 6469 lb., and maximum airspeed  $V_{max}$  of 109 knots true airspeed (KTAS). The L+C is a turboelectric variant, with eight two-bladed lifting rotors, a three-bladed pusher propeller, gross weight of 5903 lb., and  $V_{max}$  of 123 KTAS. Additional details on these configurations can be found in Silva et al.<sup>8</sup>



Figure 1: NASA RVLT reference vehicle configurations considered in this study: quadrotor (left) and lift plus cruise (right).

### B. Operating States

Trajectory data from a set of operational scenarios with multiple vertiports were used in the Gen 1 and Gen 2 analyses. These data were reduced to determine aircraft operational states for which noise estimates are needed. In this paper, the aircraft operating states are defined by pairs of airspeed (knots) and climb angle (degrees). These comprise 42 and 44 unique operating states for the quadrotor and L+C vehicles, respectively, and are binned in 10 knot increments of airspeed (from 0 to 85% of  $V_{max}$ ) and in  $5^\circ$  increments of climb angle (from  $-90^\circ$  in vertical descent, to  $90^\circ$  in vertical ascent). Because the source noise prediction process can be computationally intensive, only those operating states having at least 10 occurrences in the Gen 1 trajectory data were evaluated. The set of Gen 1 operating states was compared with operating state data derived from the Gen 2 trajectory data and was found to adequately cover the range of conditions, see Figure 2. Source noise data for operating states with airspeeds less than 5 knots were computed with zero airspeed, irrespective of climb angle.

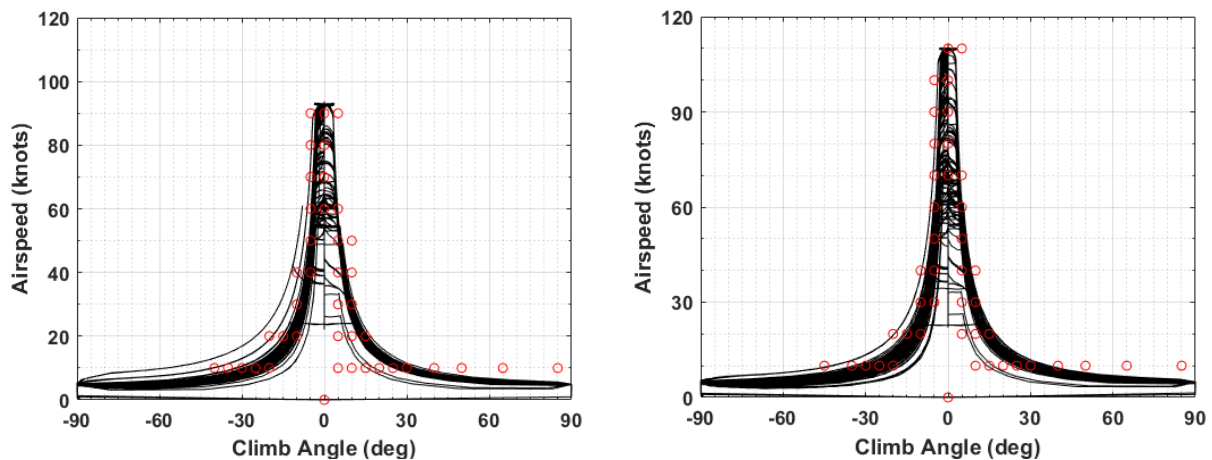


Figure 2: Operating states for the quadrotor (left) and L+C (right) vehicles. Black lines represent operating states derived from the Gen 2 trajectory data and red circles represent states identified in the Gen 1 study.

For the Gen 3 NPD database, an additional operating state corresponding to the rotary-wing “Flight Idle” operational mode is required for both vehicles, see Section IV.B. Although not occurring in the Gen 1 or Gen 2 trajectory data, either this state or the “Ground Idle” state is required in the database for modeling rotary-wing departure profiles within AEDT.

### III. Source Noise Prediction Process

This section reviews the process for generating source noise data through analysis, including determination of trimmed conditions for each vehicle. The source noise data are subsequently used for generation of both fixed-wing and rotary-wing NPD data. A summary of each analysis step follows. The overall process is depicted in Figure 3, in which the script “pyaaron” executes all steps for each operating state.

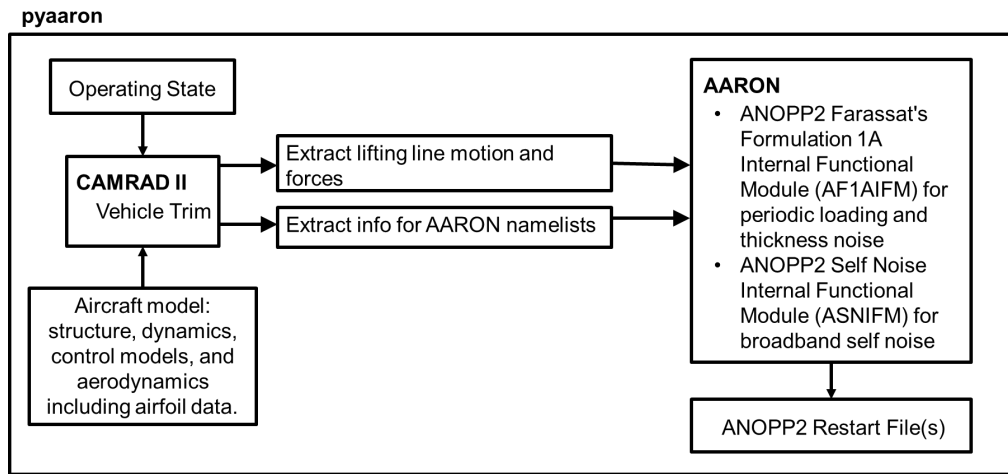


Figure 3: NASA process for generating source noise data for each operating state.

#### A. Vehicle Trim

For a given vehicle (quadrotor or L+C) and prescribed operating state, the vehicle is “trimmed” in an iterative process using a comprehensive analysis code. For this work, the Comprehensive Analytical Model of Rotorcraft Aerodynamics and Dynamics (CAMRAD II)<sup>2</sup> computer program is used to trim the vehicles. In the trimmed condition, the control surface configuration of the vehicle corresponds to the desired operating state (airspeed and climb angle). CAMRAD II provides the lifting line geometry and motion to both the compact loading and compact thickness models and the forces acting on the lifting line to the compact loading model, see Section III.B. CAMRAD II also provides the angle of attack and the three components of wake-induced fluid velocity as a function of rotor blade radial station and azimuth. These serve as inputs to source noise prediction modules explained below.

##### Quadrotor Vehicle Trim

The rotors on the quadrotor vehicle operate at a constant RPM with a 20 Hz blade passage frequency (BPF) and utilize collective pitch control. The six trim targets for the six-degree-of-freedom (6 DOF) trim are the three net forces and three net moments ( $F_x$ ,  $F_y$ ,  $F_z$ ,  $M_x$ ,  $M_y$ , and  $M_z$ ) in the aircraft coordinate system acting on the aircraft center of gravity (CG). Four of the six trim variables are four pilot controls: collective stick, lateral stick, longitudinal stick, and pedal. These pilot controls (variables) are connected to appropriate combinations of the four rotors’ collective pitch settings. The remaining two trim variables involve two vehicle orientation angles: vehicle pitch and vehicle roll. This same 6 DOF trim method is used for all speed and climb angle combinations. For flight idle (used when modeling aircraft in AEDT as rotary-wing vehicles), the vehicle rests on the ground and the net vertical force,  $F_z$ , is trimmed to 80% of the vehicle weight with the trim variable being pilot collective stick. All other motion of the vehicle is restricted to zero. Furthermore, the ground effect model of CAMRAD II is enabled. This model incorporates the effect of the ground on the free wake geometry by using an image plane and the effect of one rotor’s wake on the others. This free wake geometry, altered by the presence of the ground and the other rotors as shown in Figure 4, affects the trim and blade loading.

### L+C Vehicle Trim

The lifting rotors and pusher propeller on the L+C vehicle also operate at a constant RPM (35 Hz BPF for lifting rotors, 127 Hz BPF for propeller) and utilize collective pitch control. However, different trim variables and trim targets are used depending on the flight conditions. At low speeds, the pusher propeller is not used as a trim variable. The trim targets are three degrees-of-freedom for longitudinal trim ( $F_x$ ,  $F_z$ , and  $M_y$ ). Two of the three trim variables are pilot controls: collective stick and longitudinal stick; the third trim variable is the vehicle pitch angle. At moderate speeds, all lifting rotors and the pusher propeller are active. The trim targets are the same as those used at low speed; however, the third trim variable is the pusher collective pitch instead of the vehicle pitch orientation. In this case, the vehicle pitch orientation is set to zero. At high-speed (cruise) conditions, the lifting rotors are turned off, and the wing produces lift, with thrust provided by the pusher propeller. The trim targets are two degrees-of-freedom for longitudinal trim ( $F_x$  and  $F_z$ ), and trim variables include the pusher collective pitch and vehicle pitch orientation. The dividing lines between trim modes are determined by several factors related to the operating state. For flight idle, the vehicle is trimmed in ground effect in the same manner as the quadrotor vehicle except that, like the low-speed scheme, the pusher propeller is not used. Wake interactions are shown in Figure 4.

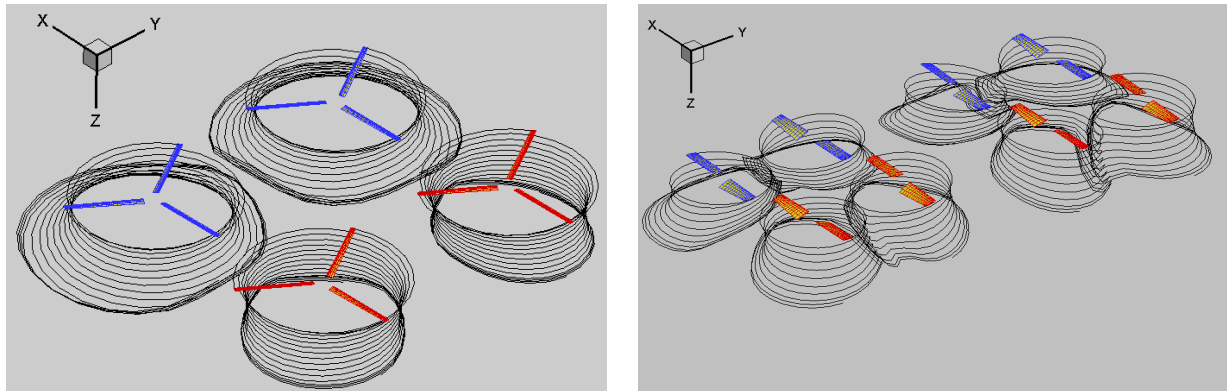


Figure 4: Interaction of free wakes with ground plane and each other for quadrotor (left) and L+C vehicles (right) in ground idle mode. Front rotors are in blue and aft rotors are in red and the positive z-direction is down.

### **B. Source Noise Definition**

Source noise data are generated using ANOPP2's Aeroacoustic Rotor Noise (AARON) tool. Two noise sources are included in the Gen 3 database. Farassat's Formulation 1A,<sup>10</sup> incorporated in ANOPP2's Formulation 1A Internal Functional Module (AF1AIFM),<sup>11</sup> is used to compute the periodic loading and thickness noise components under each quasistatic operating condition. For all source noise calculations in this paper, the compact thickness and compact loading version of AF1AIFM is used.<sup>12</sup> For compact thickness, the user provides the cross-sectional area of the blade section as a function of blade radius. In pyaaron, the user provides maximum thickness to chord ratio at radial stations and the cross-sectional area is computed assuming a NACA 00XX airfoil section, where XX is the thickness-to-chord ratio in percent. CAMRAD II input, discussed in Section III.A, is used for compact loading noise computations.

Broadband self noise data are generated using ANOPP2's Self Noise Internal Functional Module (ASNIFM), following the semiempirical formulations by Brooks et al.<sup>13</sup> Additional input data for the self noise analyses, apart from the CAMRAD II output, include the zero-lift angle of attack as a function of rotor radius and the trailing edge (TE) thickness and TE wedge angle as a function of rotor radius. The vehicle sizing process using the NASA Design and Analysis of Rotorcraft (NDARC) code<sup>14</sup> specified the lifting rotor and cruise propeller blades to use a Sikorsky SSC-A09 rotorcraft airfoil table for the inboard section ( $0 \leq r/R \leq 0.85$ ), a Boeing-Vertol VR-12 rotorcraft airfoil table for the outboard section ( $0.95 \leq r/R \leq 1$ ), with an interpolation between those airfoil tables for intermediate stations ( $0.85 \leq r/R \leq 0.95$ ). The zero-lift angle, shown in Figure 5, was calculated under a hover condition as a function of Mach number at each radial station. The sensitivity of the self noise calculation to the zero-lift angle has not been thoroughly investigated, so no effort was undertaken as part of this study to incorporate an azimuthal variation that would accompany any of the forward flight conditions. The TE thicknesses and wedge angles were not specified as part of the NDARC or CAMRAD II analyses. A constant TE thickness (scaled by rotor radius) and a constant TE wedge angle were specified based on representative data from the HART II rotor,<sup>15</sup> see Table 1. Since the self noise calculation is known to be sensitive to these TE parameters, the resulting self noise data are not considered to be generally applicable to other airfoil geometries.

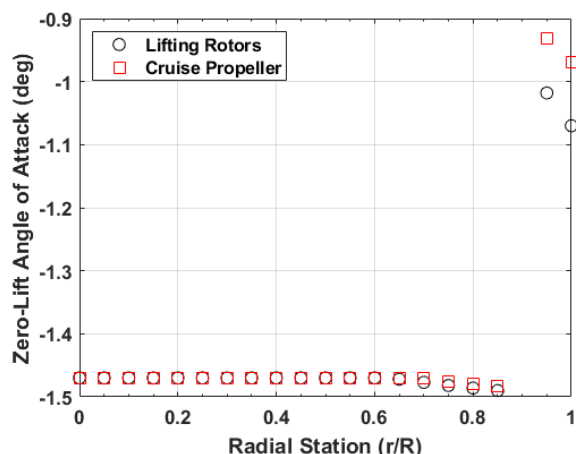


Figure 5: Zero-lift angle of attack used in the calculation of the broadband self noise component.

Table 1: Additional parameters used in the calculation of the broadband self noise component.

Rotor	TE thickness in. (mm)	TE wedge angle deg.
Quad Lifting Rotor	0.071 (1.8)	18
L+C Lifting Rotor	0.027 (0.69)	18
L+C Cruise Propeller	0.024 (0.62)	18

Source noise data generated by AARON for each operating state are provided on a hemisphere of observers centered about the CG of each vehicle at  $10^\circ$  increments in polar angle (fore-aft) and azimuthal angle (port-starboard) and at a radius of 500 ft. (100 times the lifting rotor radii of the L+C vehicle and about 38 times the rotor radii of the quadrotor vehicle) in order to ensure that the hemisphere contained only far field noise. The set of observers on the hemisphere move with the vehicle, and therefore, do not include the Doppler frequency shift that would be experienced by a stationary ground observer. The source noise data are written to ANOPP2 restart files for subsequent calculation of NPD data. Example loading and thickness noise and broadband self noise data for the quadrotor vehicle are shown in Figure 6 for a high-speed cruise condition. The loading and thickness noise is highly directional, whereas the broadband self noise is more uniformly distributed and is characterized by an overall dipole shape.

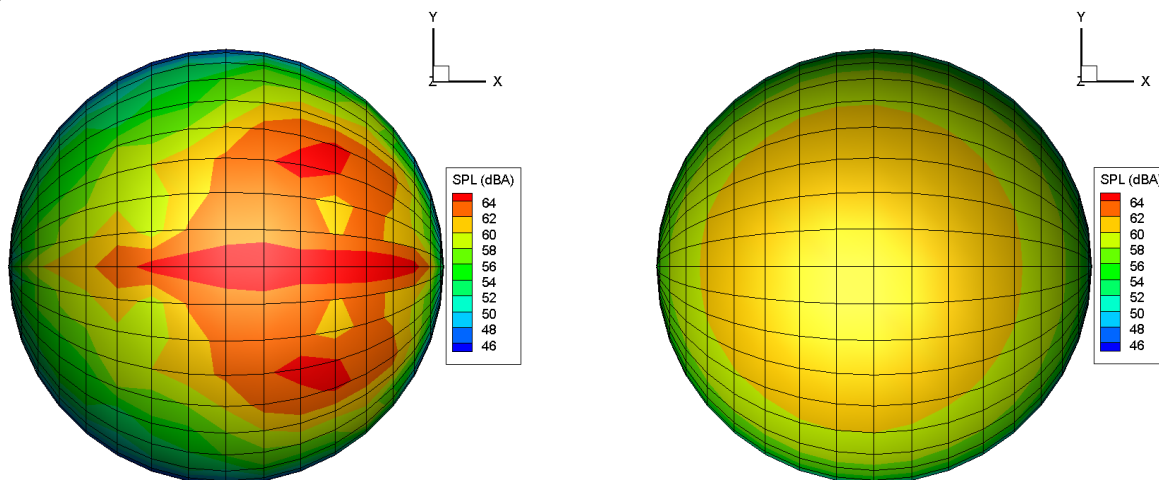


Figure 6: A-weighted overall sound pressure level (SPL) of quadrotor loading and thickness noise (left) and broadband self noise (right) for high-speed cruise. Nose is in the positive x-direction, with positive z-direction up.

#### IV. Noise-Power-Distance Data Generation

The notion of deriving NPD data from computational analysis is not new. Synodinos et al.<sup>16</sup> developed a framework for calculating NPD data for novel fixed-wing aircraft by considering changes in aircraft technology and/or operations to a baseline vehicle and operating condition. In the present work, NPD data are generated in an absolute sense, that is, not as a change to a baseline vehicle and operating condition. All NPD data for the quadrotor and L+C vehicles, whether represented as the fixed-wing aircraft type or the rotary-wing aircraft type, are derived from the same set of source noise data. In the typical AEDT analysis, each set of NPD data consists of a set of noise

metrics as a function of distance and power (fixed-wing) or operational mode (rotary-wing). For fixed-wing aircraft and rotary-wing aircraft in dynamic operational modes (see Section IV.B), these include maximum metrics (the maximum A-weighted sound pressure level  $L_{A_{mx}}$  and the maximum tone-corrected perceived noise level  $L_{PNTS_{mx}}$ ), and time-integrated exposure metrics (the A-weighted sound exposure level  $L_{AE}$  and the effective tone-corrected perceived noise level  $L_{EPN}$ ). For rotary-wing aircraft in static operational modes, these include only the maximum metrics, with exposure metrics calculated within AEDT based on the user-specified duration. Each metric is calculated at the AEDT distances (the “distance” in NPD) of 200, 400, 630, 1k, 2k, 4k, 6.3k, 10k, 16k, and 25k ft. Note that the AEDT distances reflect the slant range between the source and the receiver. The different processes for NPD data generation used for the different aircraft types are discussed next.

### A. Fixed-Wing Aircraft

AEDT permits an NPD data set for each of its three fixed-wing operational modes (approach, departure, and level flight). In a typical fixed-wing analysis, a set of procedural steps is used to specify an aircraft operation. For example, a standard approach operation is constructed as a sequence of “descent” procedural steps with increasing flap deployment and decreasing speed, followed by “landing” and “deceleration” steps. AEDT uses one of its performance models to determine the corrected net thrust per engine (the “power” in NPD) required for each procedural step and constructs a flight profile consisting of the distance along the ground track, the aircraft altitude above field elevation, the aircraft true airspeed, and the corrected net thrust. AEDT interpolates NPD data on power and distance, and applies various adjustments<sup>1</sup> to determine the noise at a set of ground receptors. This approach does not work well for UAM aircraft because flight performance model data do not exist in the Aircraft Noise and Performance (ANP)<sup>17</sup> and Base of Aircraft Data (BADA) 3<sup>18</sup> databases used in AEDT. Consequently, there are no means to determine the power required for a particular procedural step. Even then, it has not been established if the corrected net thrust of the engines is a good predictor of UAM aircraft noise levels.

An alternative AEDT modeling methodology employed in the prior UAM studies<sup>5,6</sup> directly specifies the flight profile (so-called fixed-point flight profiles), bypassing the need for a performance model to determine the power for each procedural step. In that usage, a unique identifier corresponding to the operating state (function of airspeed and climb angle) is used in place of power to designate each NPD data set. This approach requires as many NPD data sets as there are operating states, and care is needed in this approach to minimize the effect of unwanted interpolation of NPD data between unrelated operating states.<sup>5</sup>

When using fixed-point flight profiles, the computational process used to generate fixed-wing NPD data for each operating state is shown in Figure 7. Following the loading of an ANOPP2 restart file (containing the source noise data associated with a single operating state), Doppler frequency shift is applied using ANOPP2’s Wind Tunnel and Flight Effects Internal Functional Module (AWTFEIFM). For each AEDT distance, the resulting data are propagated to a 4 ft. centerline microphone location using ANOPP2’s Straight Ray Propagation Internal Functional Module (ASRPIFM). The source noise data are “flown” via simulation along a straight and level flight path at the AEDT reference speed of 160 knots, irrespective of the flight speed and climb angle associated with the particular operational state, as depicted in Figure 8. By specifying uniform atmospheric conditions, different slant range distances,  $d$ , may be computed by a simple change in altitude. A receiver time interval of 0.5 s is used in ASRPIFM to generate a set of 1/3 octave band SPL spectral data at the ground observer, and noise metrics are calculated using ANOPP2’s Acoustic Analysis Utility (AAAU). In this application, AAAU is set to include tones below 800 Hz in the calculation of  $L_{PNTS}$  (and hence  $L_{EPN}$ ) because of the low blade passage frequencies of both vehicles. The process depicted in Figure 7 is incorporated into the ANOPP2 Mission Analysis Tool (AMAT).

In this work, ASRPIFM employs the SAE ARP 866A<sup>19</sup> atmospheric absorption model, using the Chien-Soroka ground plane reflection model<sup>20</sup> with the Delany-Bazley finite impedance model<sup>21</sup> for soft ground. In the current implementation, AMAT uses the single emission angle approach in which the directivity angles associated with the ground-reflected ray are the same as those associated with the direct ray, and spherical spreading and atmospheric absorption are the same for both ground-reflected and direct rays.<sup>4</sup> The infinitely long flight path assumed by the path segmentation modeling approach<sup>22</sup> used in AEDT is effectively achieved by ensuring the finite path length used in the simulation is sufficiently long to obtain both the maximum level metrics and the time-integrated exposure metrics between the 10 dB down points on either side of the maximum level. For the latter, the minimum simulation path length increases with increasing distance. Along with other AEDT noise adjustments, speed adjustments are applied to the exposure metrics to compensate for the difference between the AEDT fixed-wing reference speed of 160 knots and the airspeed associated with the particular operating state.<sup>1</sup>

While AEDT v3d allows user-specified spectral data and while the computational approach described herein can generate such data, no attempt to do so is made in this work. Consequently, AEDT metric calculations and

adjustments requiring the use of spectral data, e.g., C-weighted metrics or changes to atmospheric absorption type, should not be undertaken.

**AMAT**

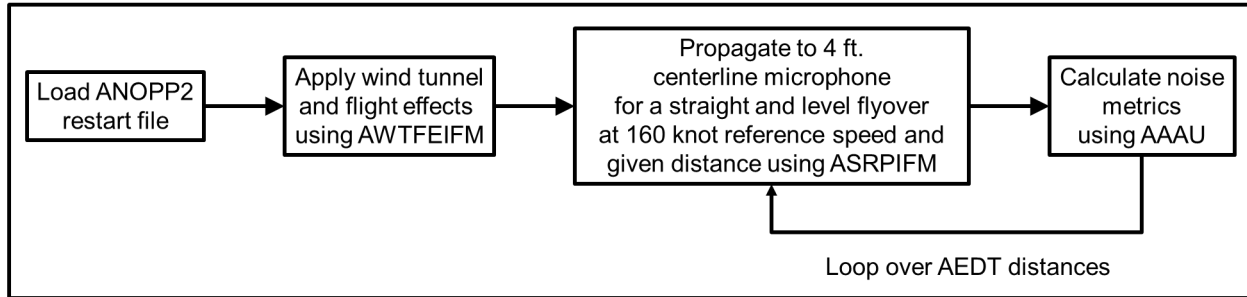


Figure 7: Computational steps in AMAT for generating fixed-wing NPD data for each operating state.

It should be noted that the NPD data generation method described above, in essence, follows that of SAE AIR 1845A<sup>23</sup> using the “integrated procedure” with Type 1 data. However, instead of measuring one set of NPD data at a nominal distance (between 100-800 m) and extrapolating to the other AEDT distances (per AIR 1845A), the current method directly computes the data at all AEDT distances. This avoids use of the “simplified adjustment procedure” in AIR 1845A for extrapolation to distances greater than 800 m. The simplified procedure employs an empirically derived duration adjustment that likely does not apply to UAM vehicles and assumes the emission angle corresponding to  $L_{Amx}$  is unchanged for distances greater than 800 m.

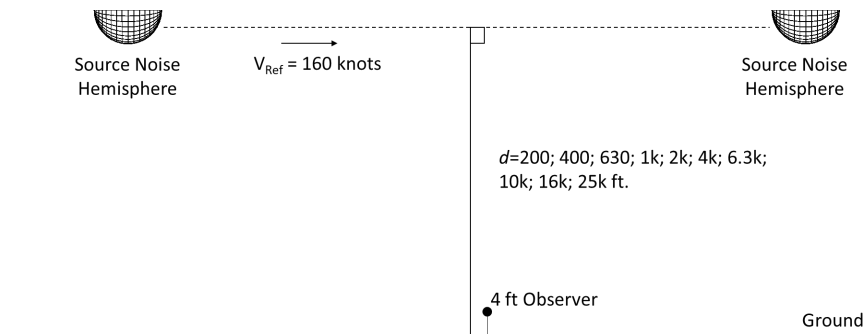


Figure 8: Simulation scenario for generating fixed-wing NPD data for each operating state.

**B. Rotary-Wing Aircraft**

In contrast to fixed-wing aircraft, in which flight profile data can be input either through a set of procedural steps or as fixed-points, flight profile data for rotary-wing aircraft can only be specified through a set of procedural steps. These procedural steps are similar to fixed-wing fixed-point flight profiles in that they do not require a flight performance model. Each procedural step denotes a particular operational mode. For example, a simple departure operation may be constructed from the following sequence of operational mode procedural steps: ground idle → flight idle → vertical ascent → departure with climbing acceleration → level flyover with constant speed. The noise data are specified as a function of operational mode (instead of power) and distance, though are still referred to as NPD data. As is the case for the fixed-wing NPD data described above, there are as many rotary-wing NPD data sets as there are operational modes. However, because rotary-wing NPD data are not interpolated between operational modes, the measures taken in prior work<sup>5,6</sup> to minimize the effect of interpolation between unrelated fixed-wing NPD data sets are not needed.

AEDT rotary-wing operational mode procedural steps are classified as either dynamic or static, see Table 2. AEDT will substitute modes (in some cases with mode-specific dB adjustments) for those that are missing from the NPD database, as indicated in the rightmost column in Table 2. Given that manufacturer supplied rotary-wing NPD data in AEDT are typically limited to the minimum set of five operational modes, i.e., modes A, D, L, G or H, and I or J, with 0 dB mode-specific adjustments for missing modes, only those modes and adjustments are considered herein. Even if all 16 operational modes were supplied, it is immediately apparent that some condensation of source noise data from the 40+ operating states identified above is required. Casting of the 40+ operating states shown in

Figure 2 into a relatively small number of allowable rotary-wing operational modes is driven, in part, by condensation considerations, which are treated differently depending on the mode.

Table 2: AEDT rotary-wing operational mode procedural steps.

Operational Mode	Description	State	Substitute Mode
A	Approach at constant speed	Dynamic	—
B	Approach with horizontal deceleration	Dynamic	A + Adj.
C	Approach with descending deceleration	Dynamic	A + Adj.
D	Departure at constant speed	Dynamic	—
E	Depart with horizontal acceleration	Dynamic	D + Adj.
F	Depart with climbing acceleration	Dynamic	D + Adj.
L	Level flyover at constant speed	Dynamic	—
T	Taxi at constant speed	Dynamic	H/I
G	Ground idle	Static	H
H	Flight idle	Static	G
I	Hover in ground effect	Static	J
J	Hover out of ground effect	Static	I
V	Vertical ascent in ground effect	Static	I + Adj.
W	Vertical ascent out of ground effect	Static	J + Adj.
Y	Vertical descent in ground effect	Static	I + Adj.
Z	Vertical descent out of ground effect	Static	J + Adj.

It should be noted that unlike the methods used for generating fixed-wing NPD data, essentially following AIR 1845A,<sup>23</sup> there is no standard for generating rotary-wing NPD data. To the extent possible, the methods used herein are consistent with those for helicopter certification according to 14 CFR Part 36 Appendix H.<sup>24</sup>

### 1. Dynamic Operational Modes

The computational steps for generating rotary-wing NPD data for dynamic operational modes are similar to those of fixed-wing, except for two important distinctions, see Figure 9. One is that for each dynamic mode, three sets of noise metrics are needed as a function of the AEDT reference distances: one set along the centerline and one each at  $\pm 45^\circ$  azimuth angles to represent lateral directivity, see Figure 10. The lateral directivity adjustment in AEDT interpolates NPD data for lateral emission angles between  $\pm 45^\circ$  and uses the data at  $\pm 45^\circ$  for lateral emission angles greater than  $|\pm 45^\circ|$ . The additional observers require additional simulations because the trade of altitude for distance is different between the centerline observer and the lateral observers. The other distinction is that the NPDs are calculated at the intended operating state (airspeed and climb angle), not at the reference airspeed of 160 knots in level flight used for fixed-wing aircraft. There is a different reference speed for each dynamic operational mode A, D, and L.

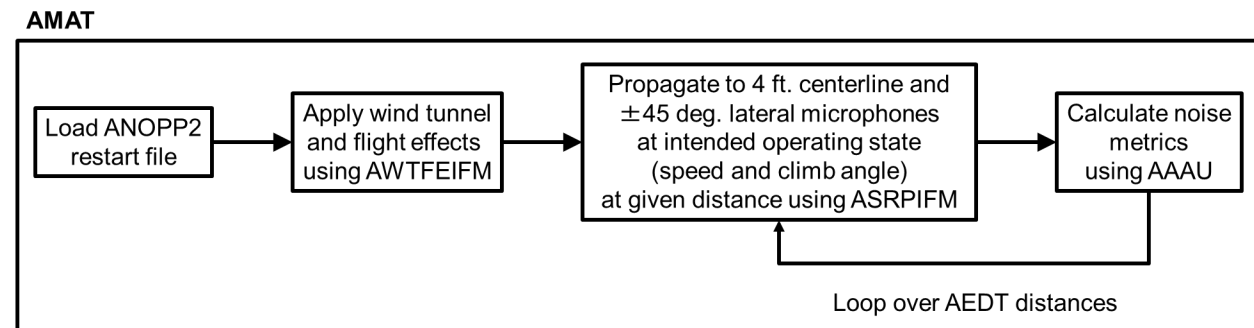


Figure 9: Computational steps in AMAT for generating rotary-wing NPD data for dynamic operational modes A, D, and L.

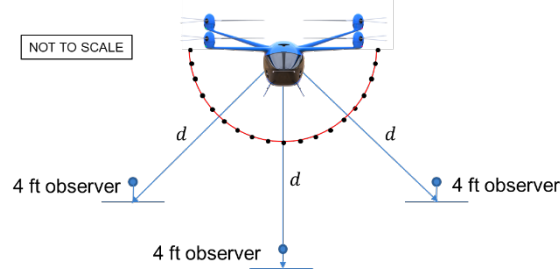


Figure 10: Lateral distribution of observers (centerline,  $\pm 45^\circ$ ) for rotary-wing dynamic operational modes.

#### Dynamic Mode L (Level Flyover at Constant Speed)

Simulation of dynamic mode L for generation of NPD data is similar to the fixed-wing simulation, as depicted in Figure 8. For both the quadrotor and L+C vehicles, there are multiple zero climb angle operating states having various nonzero airspeeds. The approach taken to condense the multiple cases down to a single mode L utilizes the AEDT source noise adjustment due to advancing tip Mach number ( $MN_{ADV}$ ). This adjustment, developed for helicopters, accounts for changes in sound level associated with changes in the rotor revolutions per minute (RPM), airspeed, and/or ambient temperature. This approach enables the mode L NPD to cover a range of flight speeds. The adjustment is described in 14 CFR Part 36 Appendix H<sup>24</sup> and examples are provided by Rickley et al.<sup>25</sup> The degree to which this adjustment applies to UAM vehicles, particularly in propeller-driven wing-borne flight, is discussed in Section V.B.

The approach is summarized as follows. First, at the 1000 ft. distance, values of  $L_{PNTS_{mx}}$  are calculated for each of the three observer locations for each of the nonzero airspeed level flight conditions. One of the airspeeds is selected as the reference airspeed for mode L. The source noise adjustment ( $\Delta dB$ ) for each of the three observers is given by

$$MN_{ADV} = B_0 + B_1(M_{ADV_T} - M_{ADV_R}) + B_2(M_{ADV_T} - M_{ADV_R})^2 \quad (1)$$

in which  $B_0$ ,  $B_1$ , and  $B_2$  are vehicle specific coefficients derived from a second order polynomial regression of  $L_{PNTS_{mx}}$  as a function of  $\Delta M_{ADV}$ , and  $M_{ADV}$  are the advancing tip Mach numbers at the operational airspeed  $V_T$  (knots) and the reference airspeed  $V_R$  (knots).  $M_{ADV}$  is the sum of the translational Mach number from the forward airspeed and the rotational blade tip Mach number, and is given by

$$M_{ADV} = \left( 1.688V + \frac{2\pi r \text{ RPM}}{60} \right) / c = \left( 1.688V + \frac{\pi d \text{ RPM}}{60} \right) / c \quad (2)$$

in which  $r$  is the blade length (ft),  $d$  is the rotor diameter (ft),  $c$  is the speed of sound in air (ft/s)  $[ = 49.018\sqrt{459.63 + T} ]$ ,  $T$  is the temperature in  $^\circ\text{F}$ , and the reference temperature is  $77^\circ\text{F}$ . The NPD data for mode L is condensed to three sets (one for each observer) of noise metrics at the ten AEDT distances for the selected reference condition, plus three sets of regression coefficients. The adjustments to the maximum noise levels and time-integrated noise exposure levels are applied within AEDT.

#### Dynamic Modes D (Departure at Constant Speed) and A (Approach at Constant Speed)

Simulations of dynamic modes D and A for generation of NPD data are depicted in Figure 11 and Figure 12, respectively. Recalling Figure 2, there are several departure operating states (having positive climb angles) and several approach operating states (having negative climb angles). The dividing line between operating states best characterized by static vertical ascent modes V/W with high climb angles and those best characterized by dynamic departure mode D with lesser climb angles lies in the realm of engineering judgement. The same argument holds for static vertical descent modes Y/Z and approach mode A. Even so, making such a distinction would still leave several operating states for each of modes D and A.

Unlike mode L, there is no advancing tip Mach number adjustment in AEDT that can aid in the condensation to a single set of NPD data for each of the modes D and A. The approach taken herein for the necessary condensation is simply to calculate metrics for every set of operating states identified as D and A, then to select one for each based on an appropriate criterion. For example, if a worst-case noise assessment was of interest, then the operating state having the highest levels could be selected. Alternatively, if a noise assessment of the average case was of interest, then the operating state best representing all NPD data could be selected. It is also feasible to perform a Monte Carlo simulation using many different vehicle variants of the same vehicle, each using a different distribution of

NPD data. The important point is that only one set of data for each mode can be specified per vehicle, and the set that is selected dictates the reference airspeed for the respective mode.

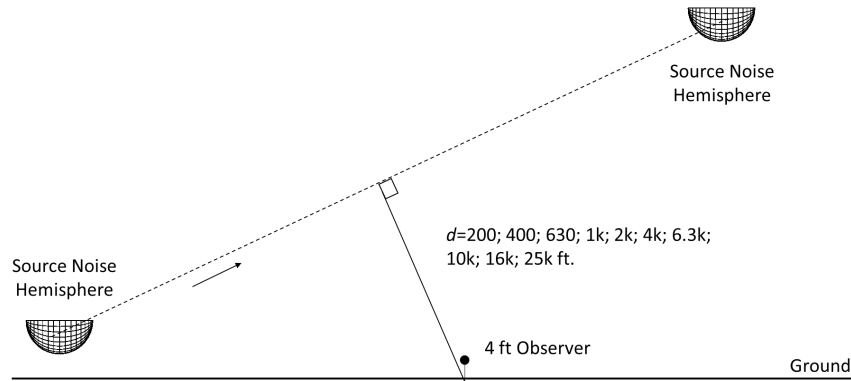


Figure 11: Simulation scenario for generating rotary-wing NPD data for dynamic mode D.

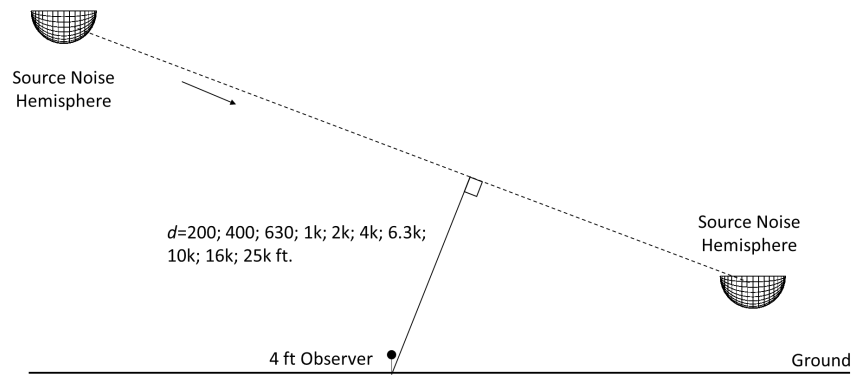


Figure 12: Simulation scenario for generating rotary-wing NPD data for dynamic mode A.

## 2. Static Operational Modes

The computational steps for generating rotary-wing NPD data for static operational modes differ from those used for fixed-wing and dynamic rotary-wing data, see Figure 13. Since the source and observer are stationary, there is no need to apply Doppler frequency shift prior to propagation. For each mode, a single set of maximum level noise metrics is provided as a function of the AEDT reference distances at locations directly in front of the vehicle. AEDT input for static modes includes the duration adjustment of the operation in order to calculate the time-integrated exposure metrics.

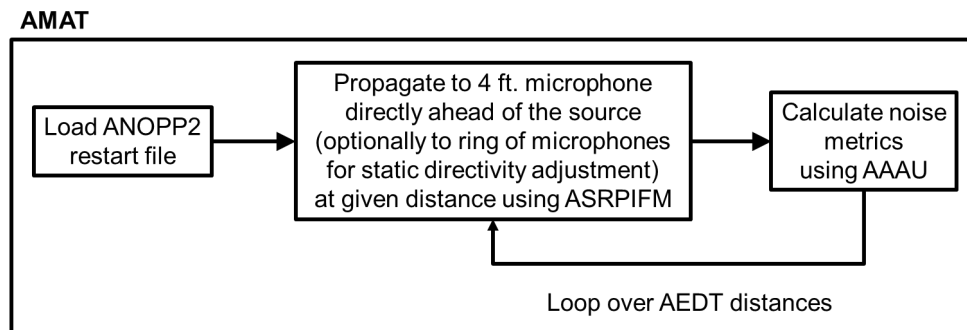


Figure 13: Computational steps in AMAT for generating rotary-wing NPD data for static operational modes G, H, I, and J.

Vehicle and mode-specific directivity adjustments may also be provided. The adjustments are specified for a single ring of azimuthal observers (in 15-45° increments) as sound levels relative to the level directly ahead of the vehicle, see Figure 14. When making ground measurements, these data are normally acquired at a 200 ft. radius.

However, since the present data are being computed, consideration of azimuthal data at other radial distances is convenient, even if for no other purpose than to assess the variation in directivity with distance. If directivity adjustment data are not provided, a 0 dB adjustment is used, making the source effectively radiate as a monopole.

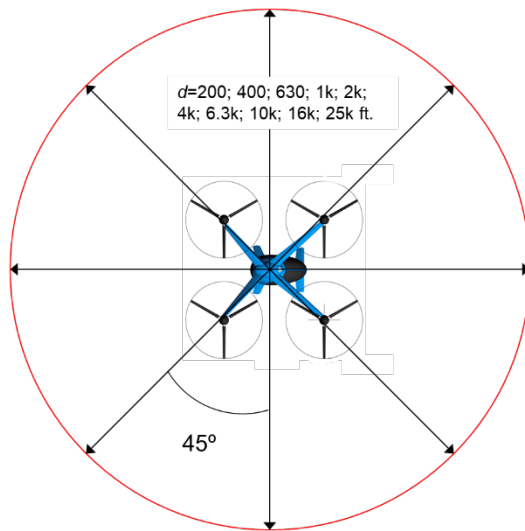


Figure 14: Static directivity adjustment data collection points for operational modes G, H, I, and J.

Directivity adjustment data may be specified separately for hard and soft ground. Note, however, that within AEDT, there are no means of selecting a ground type (hard or soft) for the static directivity adjustment independent of that used for the ground effect component of the lateral attenuation adjustment. This makes it impossible, for example, to model a takeoff and landing at a hard surfaced vertiport while accounting for ground absorption along the route, without purposefully mislabeling hard ground directivity data as soft.

#### Static Modes G (Ground Idle) and H (Flight Idle)

The method for calculating NPD data for modes G and H is the same; it is only the source noise data that differ. Given that the aircraft of interest are electrically powered, the ground idle operational mode procedural step may not be applicable. Since it is nevertheless required for rotary-wing departure operations, it will be provided by way of substitution with the flight idle step. This additional operating state, particular to rotary-wing vehicles, augments the set of operating states used for fixed-wing analyses.<sup>5,6</sup>

In this work, mode H is calculated with the aircraft CG located at the height of the 4 ft. microphone, that is, at a 0° elevation angle, with the top of the source noise hemisphere level with the microphone. Further, source directivity data are generated at all AEDT distances to determine the most representative set.

#### Static Modes I (Hover in Ground Effect) and J (Hover out of Ground Effect)

The method for calculating NPD data for modes I and J is the same; it is only the source noise data that differ. Within AEDT, the selection of mode I and J (as well as modes V and W, and modes Y and Z) is dictated by the ground effect altitude (in feet above field elevation), which is equal to 1.5 times the main rotor diameter for helicopters. If the procedural step is below the ground effect altitude, operational mode I (V and Y) will be used. Otherwise, operational mode J (W and Z) will be used. Since the applicability of the “helicopter ground effect altitude” criterion for UAM vehicles is questionable, only NPD data for mode J are calculated. When mode I is required within AEDT, it is provided by substitution, see Table 2. The operating state of zero airspeed and zero climb angle is used for mode J, see Figure 2. The corresponding source noise data were obtained with the ground effect model of CAMRAD II disabled.

Lacking a standard, mode J NPD data are calculated at a cone angle between 30-45°. The cone angle is the angle between the horizon and the observers that compose a circle of locations centered below the vehicle. For this calculation, the source noise hemisphere is positioned at an altitude equal to the AEDT distance times the sine of the cone angle. Source directivity data are obtained in 15-45° increments.

## V. Simulated NPD Data

In this section, NPD data obtained via simulation are provided for fixed-wing and rotary-wing modes, and comparisons are made where appropriate. International Standard Atmosphere conditions at sea level (1 atm pressure, 15 °C temperature, 1.225 kg/m<sup>3</sup> air density) and 70% rel. humidity were used throughout the tool chain. In the simulations, a flow resistivity of 250 kPa-s/m<sup>2</sup>, corresponding to grass, was used for the soft ground impedance.

### A. Fixed-Wing Aircraft

A comparison of simulated  $L_{AE}$  data, incorporating periodic loading and thickness noise and broadband noise, is shown in Figure 15 for the quadrotor and L+C vehicles. Here it is seen that, for cruise conditions, the quadrotor vehicle has higher levels than the L+C vehicle, as it does not benefit from lift generated by a wing. In contrast, the L+C vehicle has higher levels on takeoff and climb (departure), and, to a lesser extent, for higher speed descent conditions (arrivals) compared to the quadrotor vehicle. This is more clearly seen over the full range of AEDT distances in Figure 16 for a departure and cruise condition. Plots of the other metrics appear similar and are omitted for brevity.

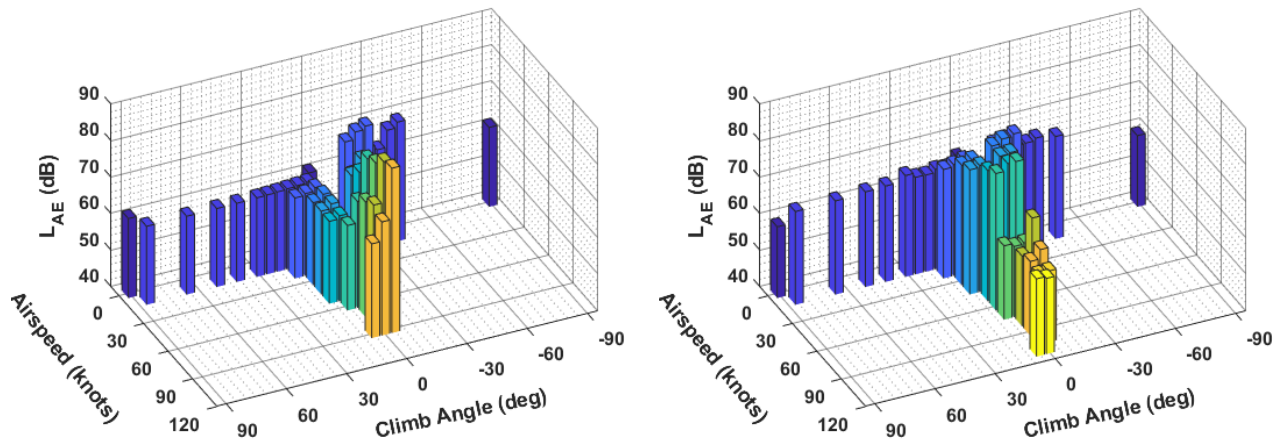


Figure 15: Simulated fixed-wing  $L_{AE}$  data for the quadrotor (left) and L+C (right) at a distance of 1000 ft.

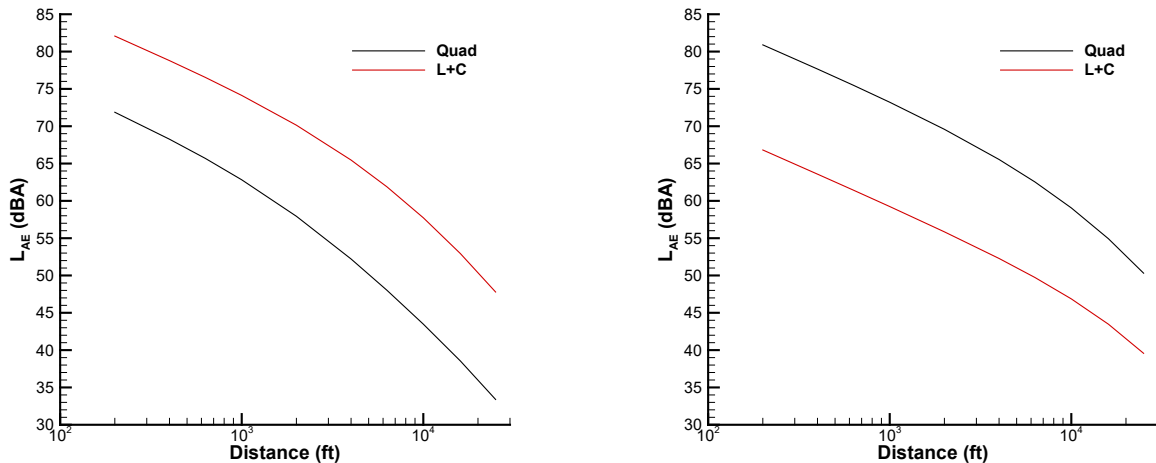


Figure 16: Simulated fixed-wing  $L_{AE}$  data for a departure operating state (40 knots, 10° climb angle) (left) and a cruise operating state (80 knots, 0° climb angle) (right).

## B. Rotary-Wing Aircraft

### 1. Dynamic Operational Modes

#### Dynamic Mode L (Level Flyover at Constant Speed)

The regression for advancing tip Mach number adjustment, using all level flyover operating states, is shown in Figure 17 for the quadrotor and L+C vehicles. According to guidance issued by the U.S. Department of Transportation, Volpe National Transportation Systems Center, if the second-order polynomial regression given by Equation (1) is not in the form of an upward curve that increases with increasing  $\Delta M_{ADV}$ , then a linear regression should be used. This was the case for all three microphone locations for the quadrotor, and for the centerline microphone for the L+C. In the case of the L+C, since the level flight operating states are fully propeller-driven, the rotational blade tip Mach number contribution to  $M_{ADV}$  in Equation (2) is zero. The simulated data for the quadrotor are symmetric with respect to the centerline, while the levels are somewhat higher on the left (port) side than the right (starboard) side for the L+C. The reference airspeeds were 70 knots and 90 knots for the quadrotor and L+C vehicles, respectively. Regression coefficients are provided in Table 3.

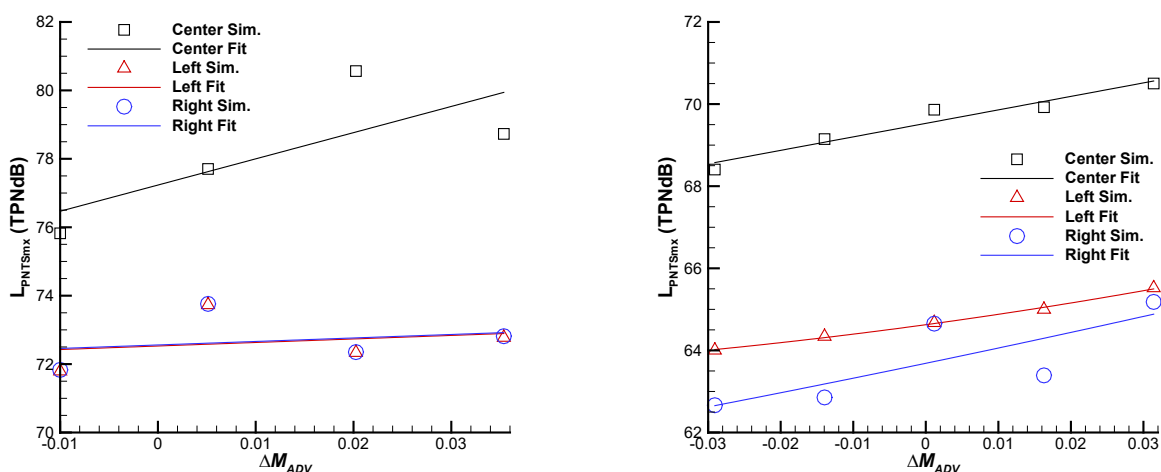


Figure 17: Regression of simulated mode L  $L_{PNTS_{max}}$  data at 1000 ft. distance for the advancing tip Mach number adjustment of quadrotor (left) and L+C (right) vehicles.

Table 3: Regression coefficients for the advancing tip Mach number adjustment.

Microphone Location	Quadrotor			Lift plus Cruise		
	$B_0$	$B_1$	$B_2$	$B_0$	$B_1$	$B_2$
Center	77.23	76.58	0	69.53	32.86	0
Left	72.53	10.31	0	64.63	24.15	114.7
Right	72.56	10.22	0	63.69	36.74	43.73

The effectiveness of this condensation can be evaluated by applying the adjustment at the appropriate  $\Delta M_{ADV}$  to the data at the reference airspeed. Figure 18 compares the simulated  $L_{AE}$  data at all level flyover airspeeds with the  $L_{AE}$  data at the reference airspeed adjusted for the advancing tip Mach number. The error between the simulated data and the adjusted data,  $\epsilon_{adj}$ , is lowest at the reference point and generally increases with increasing  $\Delta M_{ADV}$ .

An alternative condensation scheme is to select a single level flyover operating state (at the reference airspeed) and use that data for all level flyover operating states. This is the only available condensation method for modes D and A. The error between the simulated data at the reference airspeed and the simulated data at the other level flyover operating states is  $\epsilon_{ref}$ .

Which of the two condensation schemes is most effective can be judged by comparing the mean errors across the range of airspeeds. These data are provided in Table 4, where it is seen that the single level flyover operating state is marginally better than using the adjustment for all microphone positions. Further data analysis, for example using different states, is required to see if that is generally the case. The large differences seen at the right microphone position of the L+C are attributable to a greater variance in the simulated data at that location.

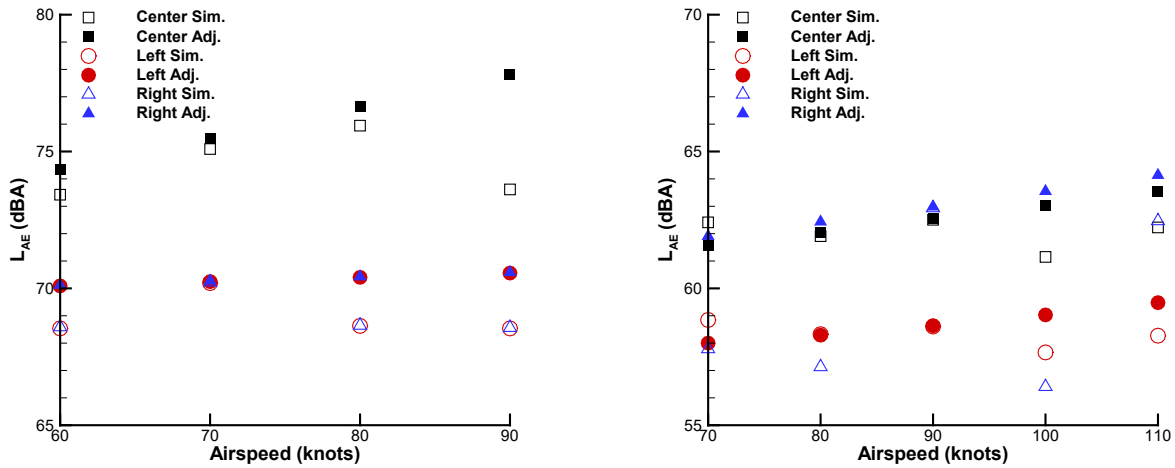


Figure 18: Simulated mode L  $L_{AE}$  data at 1000 ft. distance with reference airspeed data adjusted for advancing tip Mach number for quadrotor (left) and L+C (right) vehicles.

Table 4: Mean errors (dBA) using single dataset and using the advancing tip Mach number adjustment.

Microphone Location	Quadrotor		Lift plus Cruise	
	$\bar{\mathcal{E}}_{adj}$	$\bar{\mathcal{E}}_{ref}$	$\bar{\mathcal{E}}_{adj}$	$\bar{\mathcal{E}}_{ref}$
Center	1.5	1.0	0.85	0.46
Left	1.4	1.2	0.70	0.36
Right	1.3	1.2	3.7	3.6

#### Dynamic Mode D (Departure at Constant Speed)

Mode D NPD data were simulated for all operating states with positive climb angles of 5, 10, and 15°. The limitation on climb angles above 15° was made to ensure that the advancing side 10 dB down point needed for noise exposure metrics is met for the shorter AEDT reference distances. This is a conservative estimate made on the assumption of a monopole source and spherical spreading loss only. In the intended application, the higher climb angles will be cast as vertical ascent modes V/W, which will be substituted per Table 2 for hover modes I/J within AEDT.

Simulated mode D  $L_{AE}$  data for the quadrotor vehicle are shown in Figure 19 for centerline and 45° port side microphone locations. In these and subsequent mode D and mode A plots, the legend designates the airspeed (V) in knots and the climb angle (A) in degrees. The aims of plotting all data on a single plot are i) to identify trends and the spread in the data between operating states and microphone locations and ii) to identify outliers. Tabularized NPD data for individual operating states are not included herein. For both locations in Figure 19, the data are clustered within a range of about 9 dBA. Centerline levels are marginally higher than port side levels. Starboard side data are similar to port side data and are omitted for brevity. There is some crossover of NPD data with range, making selection of a low noise and high noise case range dependent.

Simulated mode D  $L_{AE}$  data for the L+C vehicle are shown in Figure 20 for centerline and 45° port side microphone locations. The L+C plots carry the additional designation in the legend for low speed (LS), moderate speed (MS), and high-speed (HS) trim states. As was seen in the fixed-wing NPD data in Figure 15, the levels for the high-speed trim states (in wing-borne flight) are greatly reduced from the moderate and low speed states. This indicates that the trim state should also be taken into consideration in the condensation of operating modes into a single mode D dataset, and that a grouping of these operating states with the level flight mode L might be more appropriate. In comparison to the quadrotor vehicle, at the low and moderate speed states, the L+C levels are higher and more tightly clustered, with a spread of about 2 dBA.

#### Dynamic Mode A (Approach at Constant Speed)

For a similar consideration as mode D, mode A NPD data were simulated for all operating states with descent angles 5, 10, and 15°. Within AEDT, the higher descent angles will be cast as vertical descent modes Y/Z, which will be substituted per Table 2 for hover modes I/J.

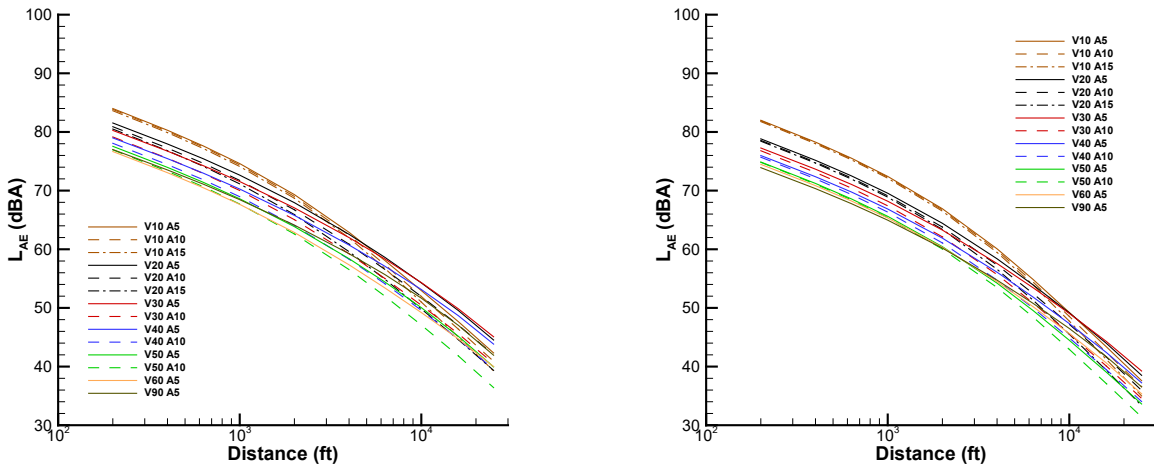


Figure 19: Simulated mode D  $L_{AE}$  data for quadrotor vehicle at centerline (left) and  $45^\circ$  port side (right) microphone locations.

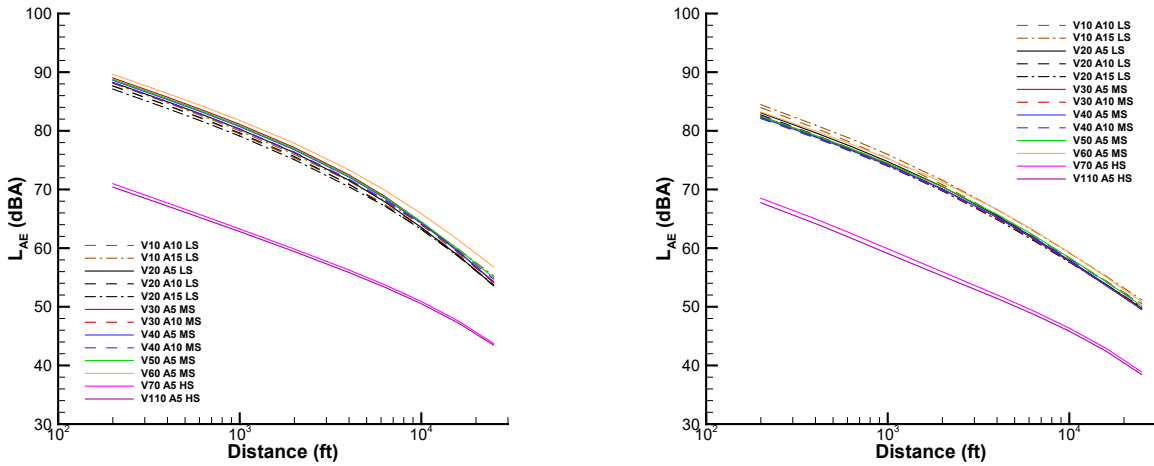


Figure 20: Simulated mode D  $L_{AE}$  data for L+C vehicle at centerline (left) and  $45^\circ$  port side (right) microphone locations.

Simulated  $L_{AE}$  data for mode A for the quadrotor vehicle are shown in Figure 21 for centerline and  $45^\circ$  port side microphone locations. In comparison to the mode D data, the mode A data are at higher levels due to induced blade-vortex interaction noise in descent. While the data are mostly parallel, the spread between the low and high noise conditions is about 12 dBA. This large range will lead to significant inaccuracies if a single mode A dataset is chosen.

Simulated mode A  $L_{AE}$  data for the L+C vehicle are shown in Figure 22 for centerline and  $45^\circ$  port side microphone locations. The lower levels associated with high speed trim (in wing-borne flight) are readily apparent and indicative that these operating states might be better grouped with the level flight mode L. Although the levels are somewhat higher than the mode D operating conditions, they are still lower than those of the quadrotor vehicle. Further, because they are mostly parallel and with a small spread, selection of a single curve that represents all mode A operating states is straightforward and does not introduce much inaccuracy.

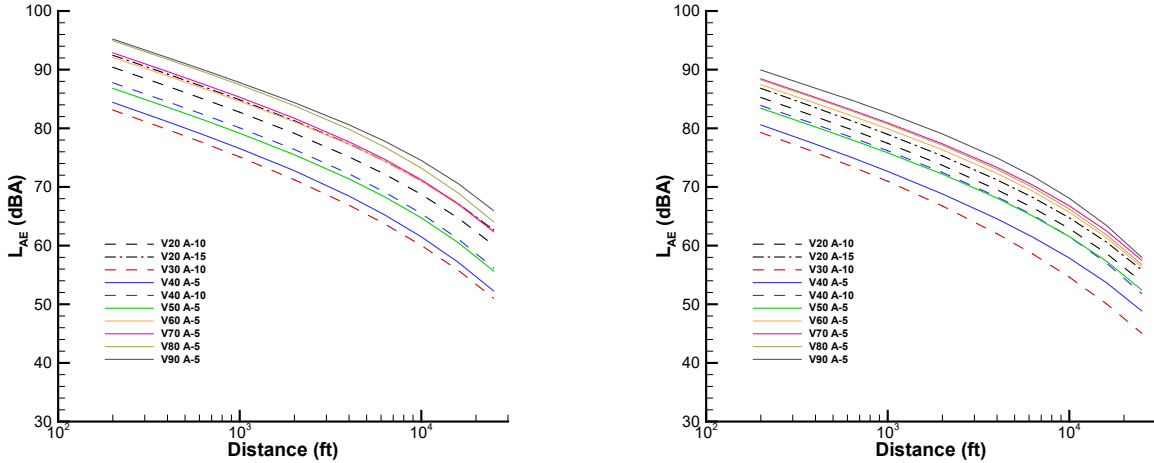


Figure 21: Simulated mode A  $L_{AE}$  data for quadrotor vehicle at centerline (left) and 45° port side (right) microphone locations.

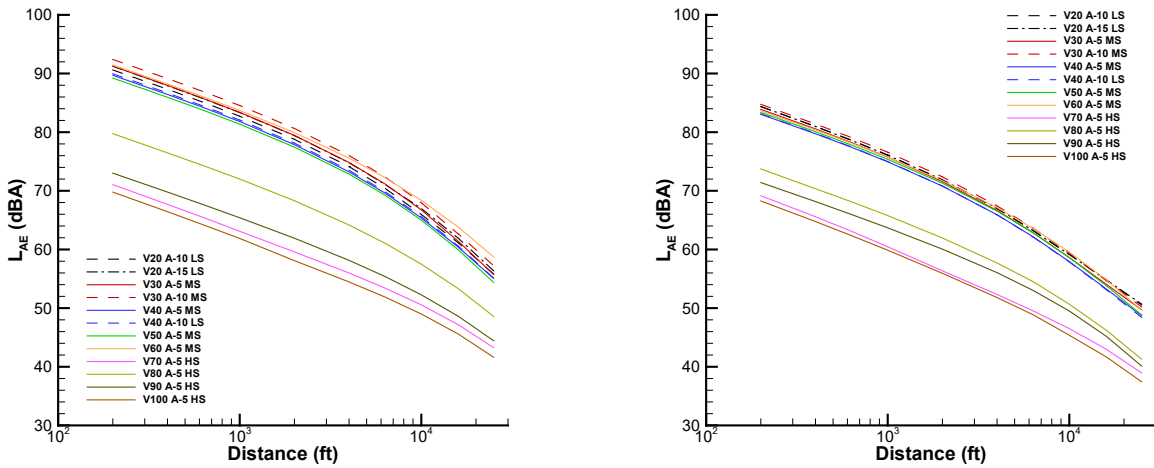


Figure 22: Simulated mode A  $L_{AE}$  data for L+C vehicle at centerline (left) and 45° port side (right) microphone locations.

## 2. Static Operational Modes

### Static Mode H (Flight Idle)

A comparison of simulated  $L_{Amx}$  data directly ahead of both vehicles is shown in Figure 23. The data were computed at a 0° elevation angle. At the time of this writing, the ground plane reflection for this operational mode was not fully verified within AMAT, so the results shown do not include that propagation effect. However, it is expected to significantly reduce levels at the grazing angles of incidence associated with this static mode. As it stands, the noise produced by the lifting rotors of the L+C vehicle is seen to exceed that of the quadrotor vehicle; the latter falls below 0 dBA at the 16k and 25k ft. distances. While there is no fixed-wing analogue to this operational mode, the higher level of the L+C vehicle is consistent with the 0 knot, 0 climb angle operating state.

The static directivity of the quadcopter vehicle is shown in Figure 24. The nose of the vehicle is at 0° and the pattern is practically symmetric about the body axis. The adjustments relative to the 0° data are also shown in Figure 24. The spiky appearance is accentuated by the 15° resolution used for AEDT. While the directivity shape does not vary much with distance, the adjustment levels increase with increasing distance. This indicates that the recommended directivity of 200 ft. substantially underestimates the adjustments at the remaining distances, particularly those in excess of 10k ft. Examination of the spectral data at the microphones (not shown for brevity) indicate that the spectral balance shifts from high frequency dominant broadband self noise to low frequency dominant loading and thickness noise as atmospheric absorption increases with increasing distance, particularly at

high frequencies. As a result, the overall levels become increasingly influenced at larger distances by differences in low frequency tonal amplitudes, which also get attenuated to varying degrees by A-weighting. In contrast, the static directivity levels for the L+C vehicle, shown in Figure 25, are higher in amplitude. However, the adjustments vary in level only by about 2 dB (between about 7 to 9 dB) over the range of distances. The spectral balance of the L+C vehicle (not shown for brevity) is dominated by low frequency loading and thickness noise. Therefore, as the broadband self noise becomes more and more attenuated with increasing distance, it does little to change the overall level. The variation is largely driven by low frequency tonal amplitudes that get attenuated to varying degrees by A-weighting.

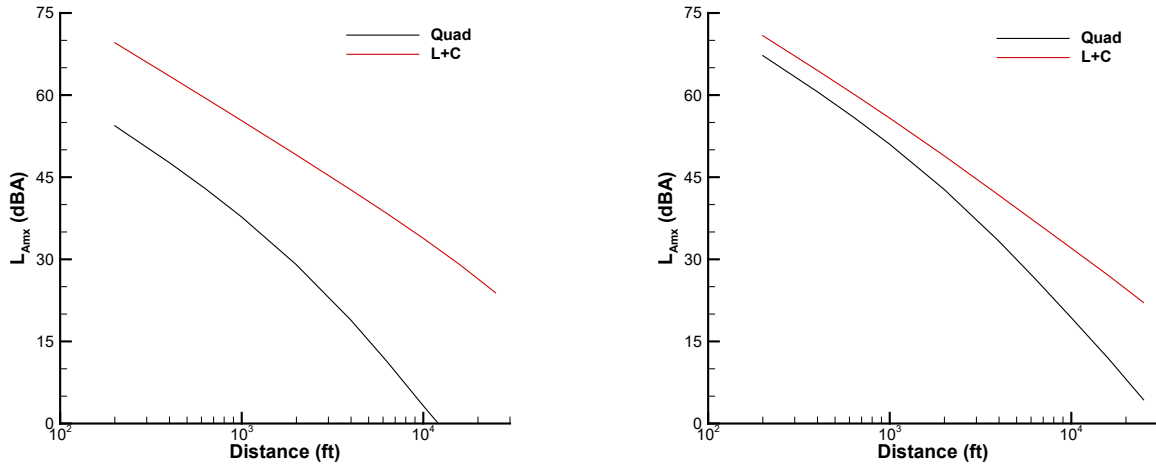


Figure 23: Simulated mode H (left) and mode J (right)  $L_{Amx}$  data for quadrotor and L+C vehicles.

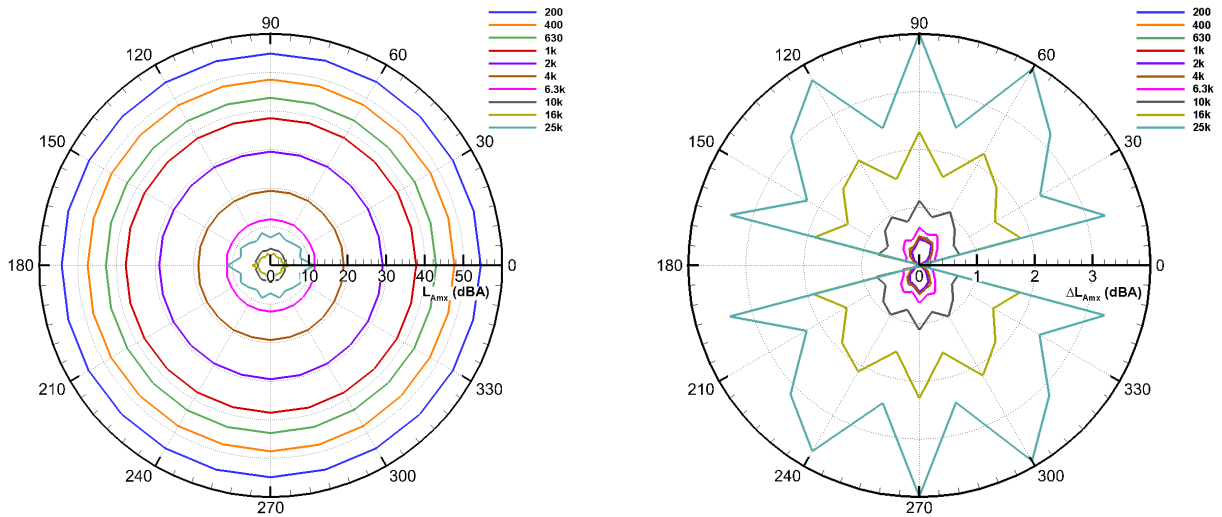


Figure 24: Mode H static directivity  $L_{Amx}$  (left) and adjustments relative to  $0^\circ$   $\Delta L_{Amx}$  (right) without ground reflection for the quadrotor vehicle.

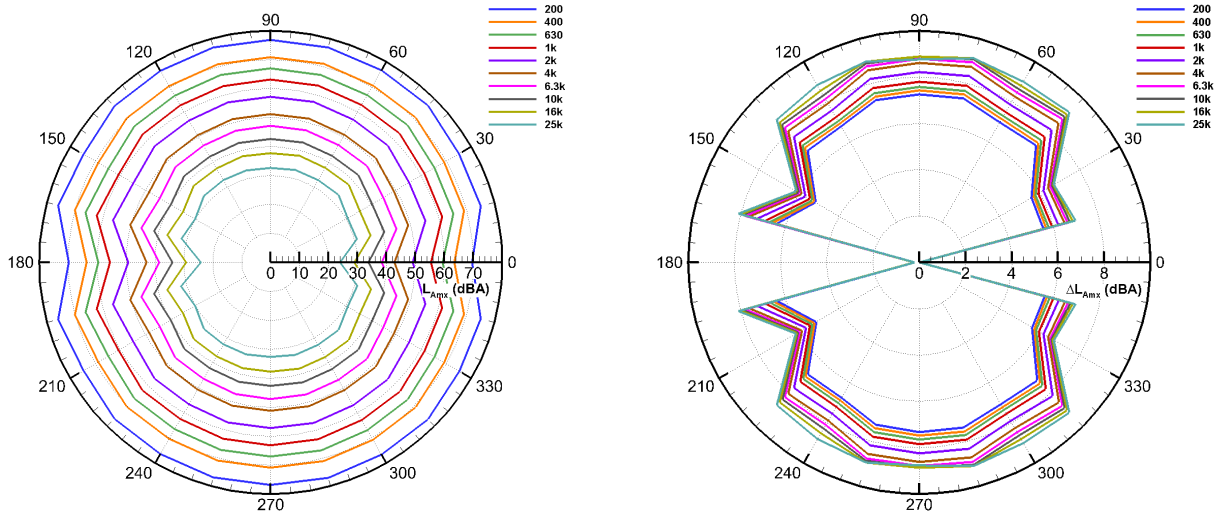


Figure 25: Mode H static directivity  $L_{Amx}$  (left) and adjustments relative to  $0^\circ$   $\Delta L_{Amx}$  (right) without ground reflection for the L+C vehicle.

Static Mode J (Hover out of Ground Effect)

A comparison of  $L_{Amx}$  data directly ahead of both vehicles is also shown in Figure 23 for static mode J. The data were computed at a cone angle of  $30^\circ$ , in the lower hemisphere region with a generally higher broadband self noise component than found at  $0^\circ$ . The data shown for this mode include the acoustic propagation effect of the ground reflection (not to be confused with the ground effect which alters the blade loading). Consistent with Figure 15, the L+C levels exceed those of the quadrotor for this condition.

The static directivity pattern and adjustments, shown in Figure 26 for the quadrotor vehicle, are again practically symmetric about the body axis. While the directivity shape does not vary much with distance, the adjustment levels increase with increasing distance, consistent with a spectral balance dominated by high frequency broadband self noise. The recommended directivity distance of 200 ft. again substantially underestimates the adjustments at the remaining distances, particularly those in excess of 1000 ft. The static directivity pattern and adjustments for the L+C vehicle are shown in Figure 27. The shapes of the adjustments are markedly different from those of the quadrotor and, as in mode H, the adjustment levels are larger than those of the quadrotor at every distance. The larger variance (about 6 dB) in adjustments (between about 2 to 8 dB), relative to the mode H data in Figure 25, is due to the larger broadband self noise contribution at this cone angle (not shown).

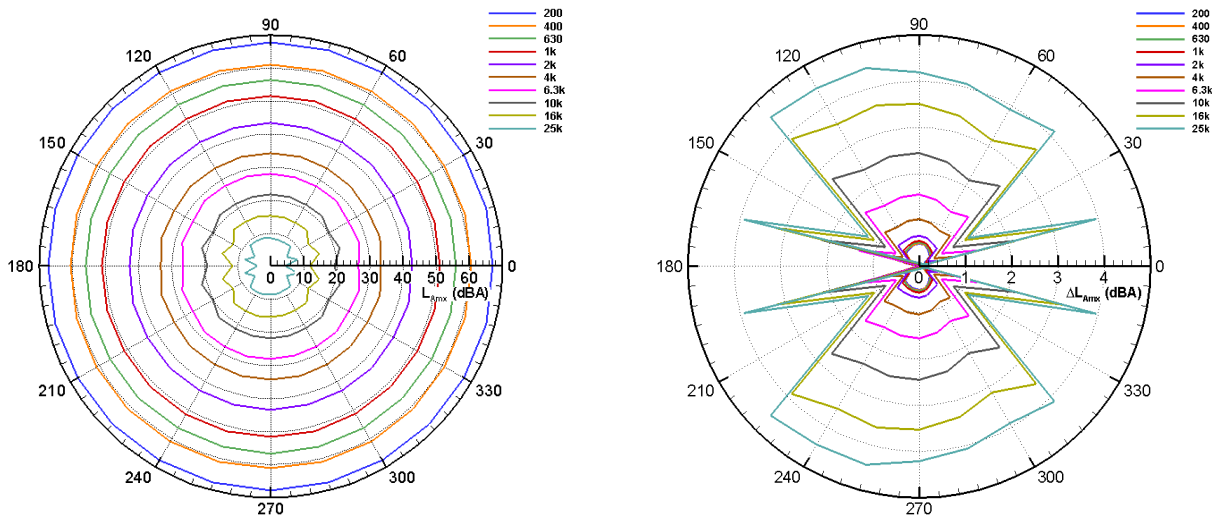


Figure 26: Mode J static directivity  $L_{Amx}$  (left) and adjustments relative to  $0^\circ$   $\Delta L_{Amx}$  (right) for the quadrotor vehicle.

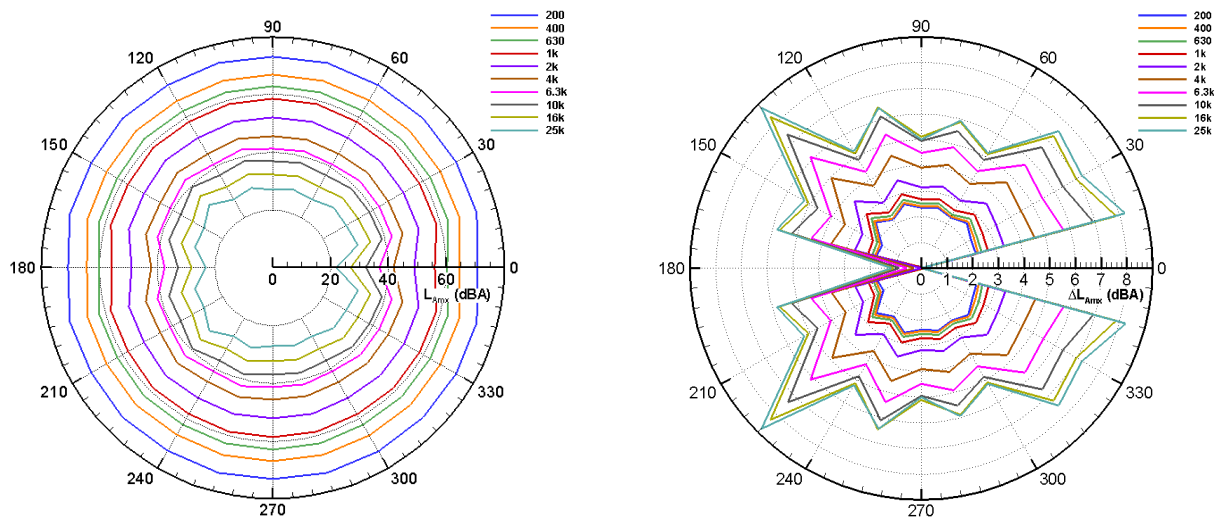


Figure 27: Mode J static directivity  $L_{Amx}$  (left) and adjustments relative to  $0^\circ$   $\Delta L_{Amx}$  (right) for the L+C vehicle.

## VI. Concluding Remarks

Methods were presented for generating noise-power-distance data from predictions of UAM vehicle source noise. The data are intended for use in the FAA AEDT computer program for studies of community noise impact from UAM flight operations. Generation of these data in this manner was necessitated by several factors including lack of UAM aircraft noise and performance data in the databases used by AEDT, and a general lack of measured UAM flight test data.

Predictions of periodic loading and thickness noise and broadband self noise were made for two reference concept vehicles that were trimmed for a range of operating states using a framework that included a comprehensive analysis code for trim and the NASA ANOPP2 for acoustic analyses. The framework is extensible to allow the inclusion of other noise sources, e.g., electric motor noise, in the future. The resulting noise hemispheres served as input to a simulation tool for generating both fixed-wing and rotary-wing NPD data, allowing the vehicles to be modeled in different ways within AEDT.

In the near term, the rotary-wing data are to be used within AEDT to model the Dallas-Ft. Worth, Texas, route structure considered in the Gen 1 study. In the longer term, AEDT modeling results using fixed-wing and rotary-wing approaches are to be compared with simulation data to identify best practices for modeling UAM operations within AEDT using fixed-wing, rotary-wing, and hybrid fixed/rotary-wing modeling approaches.

## Acknowledgments

This work was supported by the NASA Aeronautics Research Mission Directorate, Revolutionary Vertical Lift Technology Project. The authors wish to acknowledge Venkat Iyer and Jeremy Jones (Analytical Sciences and Materials, Inc.) for development of ANOPP2's Mission Analysis Tool (AMAT) used in this work. The authors also wish to thank Eric Boeker and Bradley Nicholas of the U.S. Department of Transportation Volpe National Transportation Systems Center for their consultation during the development of the methodology discussed in this paper.

## References

- <sup>1</sup>"Aviation Environmental Design Tool (AEDT) technical manual, Version 3d," U.S. Department of Transportation, Volpe National Transportation Systems Center DOT-VNTSC-FAA-21-06, Cambridge, MA, 2021.
- <sup>2</sup>Maurice, L.Q., Lee, D.S., Wuebbles, D.W., Isaksen, I., Finegold, L., Vallet, M., Pilling, M., and Spengler, J., "Assessing current scientific knowledge, uncertainties and gaps in quantifying climate change, noise and

- air quality aviation impacts," In *Final report of the International Civil Aviation Organization (ICAO) Committee on Aviation and Environmental Protection (CAEP) Workshop*, L.Q. Maurice, et al., Editors. 2009, US Federal Aviation Administration and Manchester Metropolitan University, Washington, DC and Manchester, UK.
- <sup>3</sup>Rizzi, S.A., et al., "Urban air mobility noise: Current practice, gaps, and recommendations," NASA TP-2020-5007433, 2020.
- <sup>4</sup>Lopes, L.V. and Burley, C.L., "ANOPP2 user's manual: Version 1.2," NASA TM-2016-219342, 2016.
- <sup>5</sup>Rizzi, S.A. and Rafaelof, M., "Community noise assessment of urban air mobility vehicle operations using the FAA Aviation Environmental Design Tool," *InterNoise 2021*, Virtual Meeting, 2021.
- <sup>6</sup>Rizzi, S.A. and Rafaelof, M., "Second generation UAM community noise assessment using the FAA Aviation Environmental Design Tool," *AIAA SciTech Forum*, AIAA-2022-2167, San Diego, CA, 2022, <https://arc.aiaa.org/doi/10.2514/6.2022-2167>.
- <sup>7</sup>Patterson, M.D., Antcliff, K.R., and Kohlman, L.W., "A proposed approach to studying urban air mobility missions including an initial exploration of mission requirements," *AHS International 74th Annual Forum and Technology Display*, Phoenix, AZ, 2018.
- <sup>8</sup>Silva, C., Johnson, W.R., Solis, E., Patterson, M.D., and Antcliff, K.R., "VTOL urban air mobility concept vehicles for technology development," *AIAA AVIATION Forum*, AIAA-2018-3847, Atlanta, GA, 2018, <https://doi.org/10.2514/6.2018-3847>.
- <sup>9</sup>Johnson, W.R., "Rotorcraft aerodynamic models for a comprehensive analysis," *AHS International 54th Annual Forum*, Washington, DC, 1998.
- <sup>10</sup>Farassat, F. and Succi, G., "The prediction of helicopter rotor discrete frequency noise," *Vertica*, Vol. 7, 1983, pp. 309-320.
- <sup>11</sup>Lopes, L.V., "ANOPP2's Farassat Formulations Internal Functional Modules (AFFIFMs) Reference Manual, Version 1.4," NASA TM-20210021111, 2021.
- <sup>12</sup>Lopes, L.V., "Compact Assumption Applied to Monopole Term of Farassat's Formulations," *Journal of Aircraft*, Vol. 54, No. 5, 2017, pp. 1649-1663, <https://doi.org/10.2514/1.C034048>.
- <sup>13</sup>Brooks, T.F., Pope, D.S., and Marcolini, M.A., "Airfoil self-noise and prediction," NASA RP-1218, 1989.
- <sup>14</sup>Johnson, W.R., "NDARC — NASA design and analysis of rotorcraft: validation and demonstration," *American Helicopter Society Specialists' Conference on Aeromechanics*, San Francisco, CA, 2010.
- <sup>15</sup>van der Wall, B.G., "2nd Higher Harmonic Control (HHC) Aeroacoustic Rotor Test (HART II) - Part I: Test Documentation," German Aerospace Center (DLR) IB 111-2003/31, 2003.
- <sup>16</sup>Synodinos, A.P., Self, R.H., and Torija, A.J., "Framework for Predicting Noise–Power–Distance Curves for Novel Aircraft Designs," *Journal of Aircraft*, Vol. 55, No. 2, 2018, pp. 781-791, <https://doi.org/10.2514/1.C034466>.
- <sup>17</sup>"The Aircraft Noise and Performance (ANP) Database, version 2.3," <https://www.aircraftnoisemodel.org/>,
- <sup>18</sup>"User manual for the base of aircraft data (BADA), Revision 3.15," Eurocontrol Experimental Center (EEC).
- <sup>19</sup>"SAE ARP 866 Rev. A, Standard values of atmospheric absorption as a function of temperature and humidity," SAE International, Warrendale, PA, 1975.
- <sup>20</sup>Chien, C.F. and Soroka, W.W., "Sound propagation along an impedance plane," *Journal of Sound and Vibration*, Vol. 43, No. 1, 1975, pp. 9-20, [https://doi.org/10.1016/0022-460X\(75\)90200-X](https://doi.org/10.1016/0022-460X(75)90200-X).
- <sup>21</sup>Delany, M.E. and Bazley, E.N., "Acoustical properties of fibrous absorbent materials," *Applied Acoustics*, Vol. 3, No. 2, April 1970, pp. 105-116, [http://dx.doi.org/10.1016/0003-682X\(70\)90031-9](http://dx.doi.org/10.1016/0003-682X(70)90031-9).
- <sup>22</sup>"Doc 9911, Recommended Method for Computing Noise Contours Around Airports, 2nd Edition," International Civil Aviation Organization 978-92-9258-360-6, Montreal, Canada, 2018.
- <sup>23</sup>"SAE AIR 1845A, Procedure for the Calculation of Airplane Noise in the Vicinity of Airports," SAE International Warrendale, PA, August, 2012.
- <sup>24</sup>"Noise Standards: Aircraft Type and Airworthiness Certification, CFR Title 14, Chapter 1 - Federal Aviation Administration, Department of Transportation, Part 36, Appendix H - Noise Requirements for Helicopters Under Subpart H," 2016.
- <sup>25</sup>Rickley, E.J., Jones, K.E., Keller, A.S., and Fleming, G.G., "Noise Measurement Flight Test of Five Light Helicopters," U.S. Department of Transportation, Volpe National Transportation Systems Center, DOT-VNTSC-FAA-93-5, Cambridge, MA, 1993.